A regioselectively 1, 1',3 ,3'-tetrazincated ferrocene complex displaying core and peripheral reactivity

Gordon W. Honeyman,[a] David R. Armstrong,[a] William Clegg,[b] Eva Hevia,[ac] Alan R. Kennedy,[a] Ross McLellan,[a] Samantha A. Orr,[ad] John A. Parkinson,[a] Donna L. Ramsay,[a] Stuart D. Robertson,[a*] Stephen Towie[a] and Robert E. Mulvey[a*]

a. WestCHEM, Department of Pure & Applied Chemistry, University of Strathclyde, Glasgow, G1 1XL, UK.

b. Chemistry, School of Natural and Environmental Sciences, Newcastle University, Newcastle upon Tyne, NE1 7RU, UK.

c. Current address: Department für Chemie und Biochemie, Universität Bern, CH3012, Bern, Switzerland

d. Current address: School of Chemistry, Monash University, Clayton, Melbourne, VIC 3800, Australia.

Supporting Information

Solution state study of 1

The solution phase NMR data of complex **1** solubilized in C_6D_6 showed evidence of a minor species in addition to a major form. This was based on resonance integration and the appearance of resonances at higher chemical shift in the region of the ^{1}H NMR spectrum that were consistent with protons of the Cp rings. Using 2D [^{1}H, ^{1}H] EXSY NMR spectroscopy of the solution at 298 K, clear evidence of chemical exchange emerged, initially considered to be solely through interconversion of major to minor species. On deeper investigation of this phenomenon, a further concerted structural rearrangement of the major form of the complex was revealed. It is possible to speculate that the minor form of the complex could be present for one of two reasons or both. Firstly, the minor (tentatively 'open') form of the complex could be an 'active' version of the complex which allows the bond making and breaking to occur at the Cp ring. Alternatively, the minor form of the complex could be an 'open' intermediate species which exists during the rearrangement of the major form of the complex. The minor species could also be present serving both purposes or neither. A full evaluation of these exchange processes required as complete an assignment of the ^{1}H NMR spectrum as possible (Figure S1) to allow for complete cross-peak identification to be made for the different forms of the complex in the 2D [^{1}H, ^{1}H] exchange NMR data. The data were complex owing to symmetry, chemical exchange and signal crowding in the aliphatic proton resonance region of the proton NMR data. This is a consequence of multiple TMP and *t*Bu groups with different identities. It was therefore necessary to acquire and interpret a full set of 2D [^{1}H, ^{1}H] and 2D [^{1}H, ^{13}C] correlation data alongside high resolution 1D ^{1}H and pure shift ^{1}H NMR spectra in order to track resonance identities.

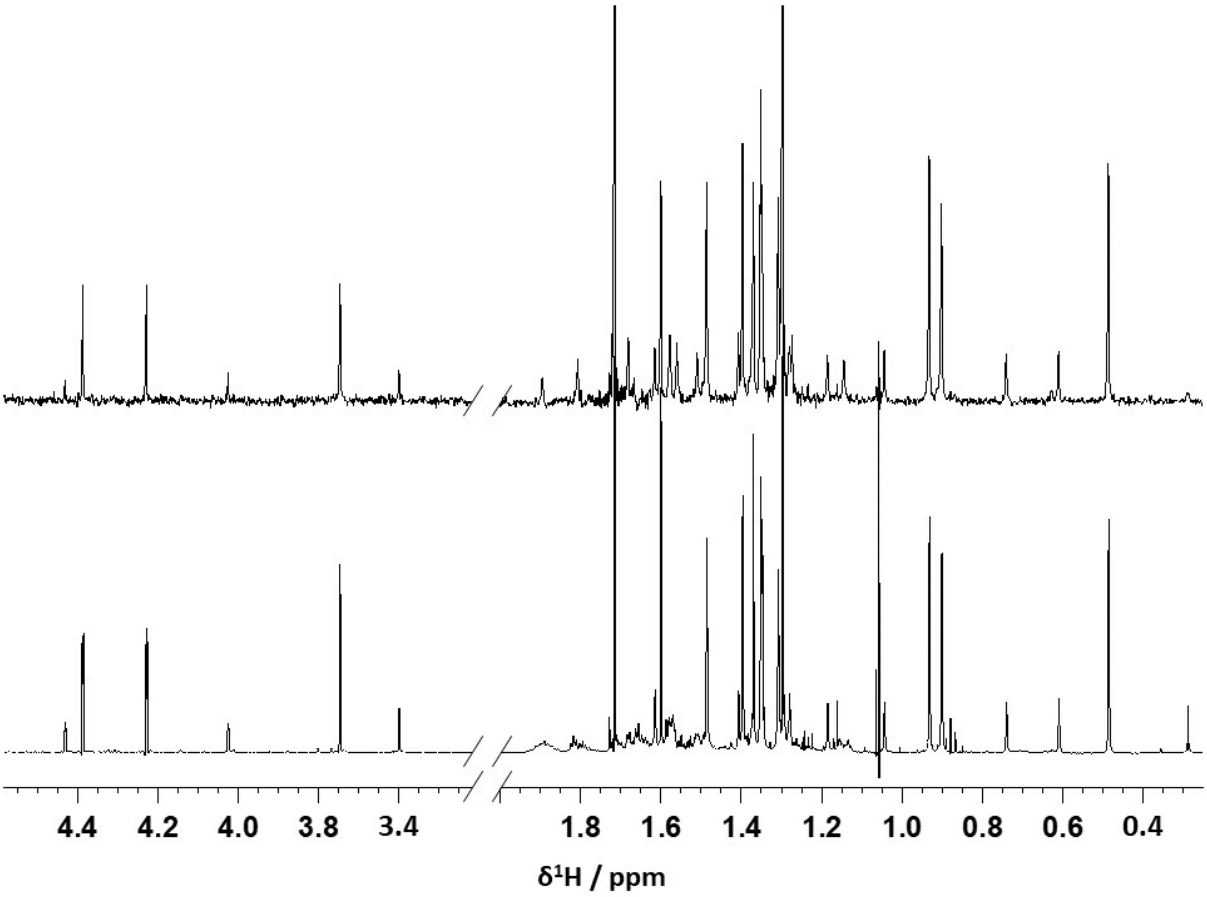

Figure S1 600 MHz 1D ^{1}H (bottom) and Pure Shift 1D ^{1}H NMR spectra (top) of the tetrametallated ferrocene complex **1**

The starting point for the ^{1}H NMR data interpretation was identification of the resonances associated with the Cp ring in the δ^{1}H = 3.50-4.50 ppm region of the spectrum. Three resonances for the major species appeared at δ^{1}H 4.387 ppm (dd, $^{3}J_{HH}$ = 1.70 Hz, $^{4}J_{HH}$ = 0.73 Hz), δ^{1}H 4.228 ppm (dd, $^{3}J_{HH}$ = 1.70 Hz, $^{4}J_{HH}$ = 1.10 Hz) and δ^{1}H 3.746 ppm (apparent t, $^{4}J_{HH}$ = 0.92 Hz representing the average $^{4}J_{HH}$ couplings of the signals at δ^{1}H = 4.387 and 4.228). The signal at δ^{1}H 3.746 ppm was assigned to H30 of the Cp ring (see Figure S2 for numbering and colouring system used within this NMR analysis) on the basis of its triplet appearance and the shared $^{4}J_{HH}$ scalar couplings. This provided the initial key that opened up access to the remaining signal assignment process.

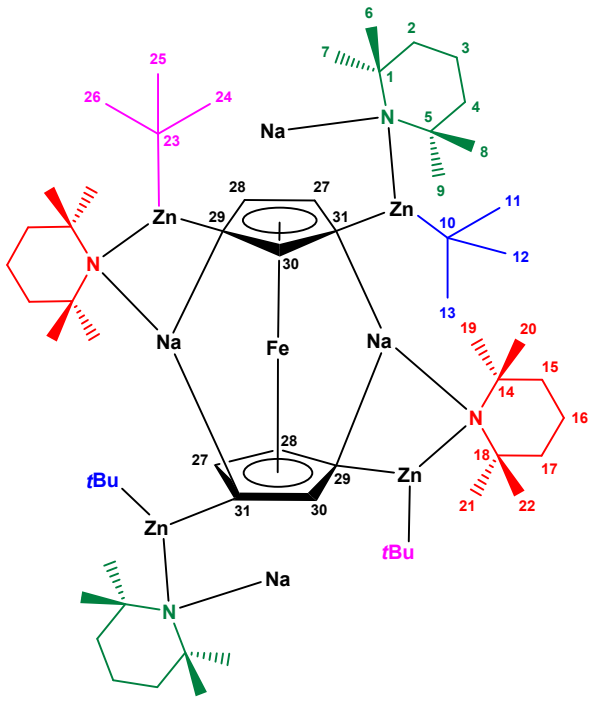

Figure S2 Atom labelling, numbering and colour scheme used with the tetrametallated ferrocene complex **1** NMR data interpretation.

Specific assignment of the two remaining ^{1}H Cp signals (H27 and H28) required close inspection of the crystal structure of the complex alongside interpretation of the nOe data. The nOe responses co-presented within the data as positive cross-peaks in the 2D [^{1}H, ^{1}H] EXSY NMR spectrum. These were present in the spectral area correlating resonances in the aliphatic region of the proton NMR spectrum with Cp ^{1}H NMR resonances. Additional, less diagnostic nOes, were also identified and ultimately assigned in other regions of the same data.

In the first instance, the assignment required stereo-specific interpretation of nOes arising from spatial interactions between protons of TMP methyl groups and Cp protons. Chemical shift considerations were used to ascribe responses to each type of TMP ring. Two types exist in the major form of the complex. For the purposes of this discussion these TMP groups are termed “capping”, TMP$_c$, and “bridging”, TMP$_b$ (these are shown colour coded, green for the former and red for the latter, in Figure S2). A strong nOe was observed between the resonance of CpH30 and a signal at δ^{1}H 1.307 ppm overlapping with a signal clearly arising from one of the two sets of as yet unassigned *t*Bu methyl groups (Figure S3, highlighted cross-peak labelled “**a**”).

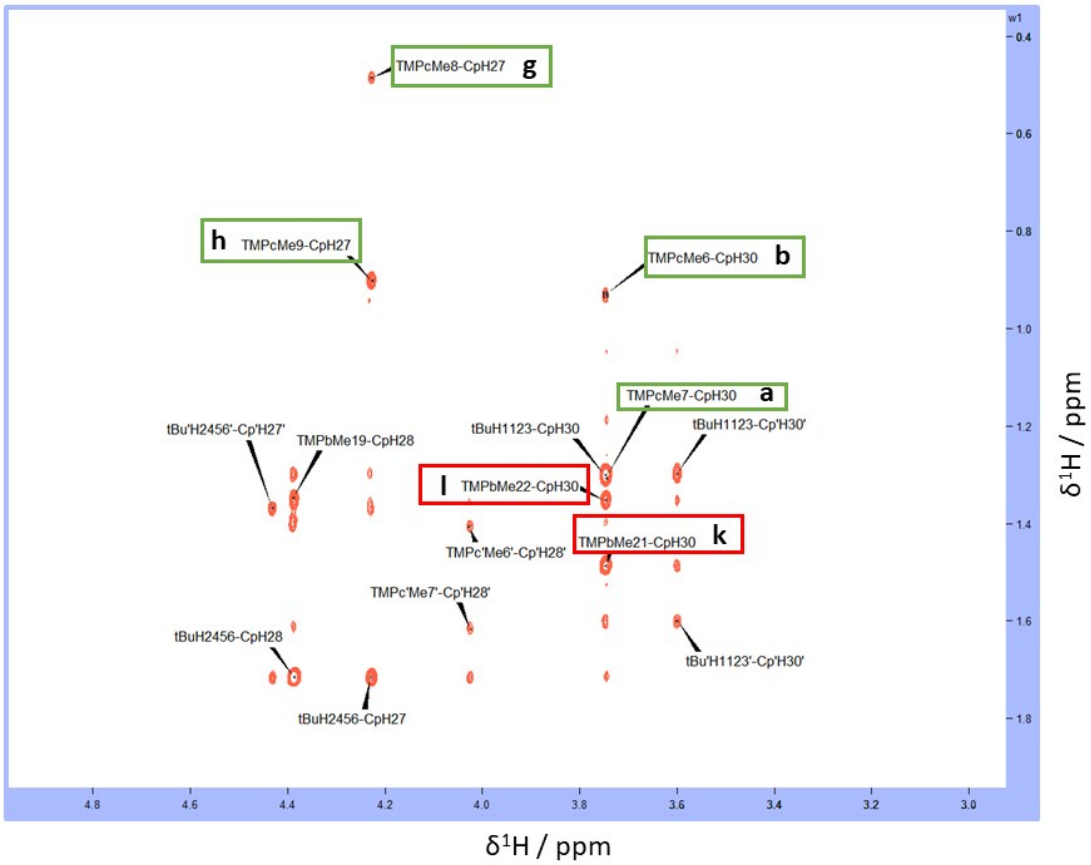

Figure S3 Region of the 600 MHz 2D [^{1}H, ^{1}H] EXSY/NOESY NMR spectrum of the tetrametallated ferrocene complex **1** showing nOes (positive peaks relative to the negatively phased data diagonal). Cross-peaks are observed between Cp protons H27, H28 and H30 to TMP and *t*Bu methyl protons. Labelling follows the convention F1 assignment (vertical chemical shift scale) followed by F2 assignment (horizontal chemical shift scale). Cross-peak labels identified inside boxes are referred to in the text by the associated letter. Colour coding: Green boxes highlight selected cross-peak assignments for the "capping" TMP_c units and red boxes highlight selected cross-peak assignments for the "bridging" TMP_b units.

A weak nOe was also observed between the CpH30 resonance and a signal at δ^1H = 0.931 ppm (Figure S3, highlighted cross-peak labelled "**b**"). 2D [^{1}H, ^{13}C] HSQC NMR data showed the signals at δ^1H 1.307 and 0.931 ppm to be $^1J_{HC}$ correlated with signals at δ^{13}C 37.23 and 34.25 ppm respectively, the shape of these signals betraying their association with methyl groups (Figure S4, highlighted cross-peaks labelled "**c**" and "**d**"). 2D [^{1}H, ^{13}C] HSQC-TOCSY and HMBC NMR data revealed these signals to also be associated with a single quaternary carbon resonance at δ^{13}C 54.28 ppm (Figure S5, highlighted cross-peaks labelled "**e**" and "**f**", tied by

a horizontal line). Interpretation of these data located the methyl groups giving rise to the signals at δ^1H 1.307 and 0.931 ppm, which are attached to the same quaternary carbon on one side of one of the two types of TMP ring. Alongside these observations, two nOes were also observed at proton chemical shift coordinates δ^1H (4.228, 0.486) ppm (weak, Figure S3, highlighted cross-peak labelled "**g**") and δ^1H (4.228, 0.902) ppm (strong, Figure S3, highlighted cross-peak labelled "**h**") between one of the two *ortho*-related Cp protons and two further TMP methyl groups. Using the same 2D [^{1}H, ^{13}C] HSQC-TOCSY/HMBC interpretation device, it was also concluded that the signals at δ^1H 0.902 and 0.486 ppm were related to one quaternary carbon signal δ^{13}C 52.52 ppm (Figure S5, highlighted cross-peaks labelled "**i**" and "**j**" tied by a horizontal tie-line).

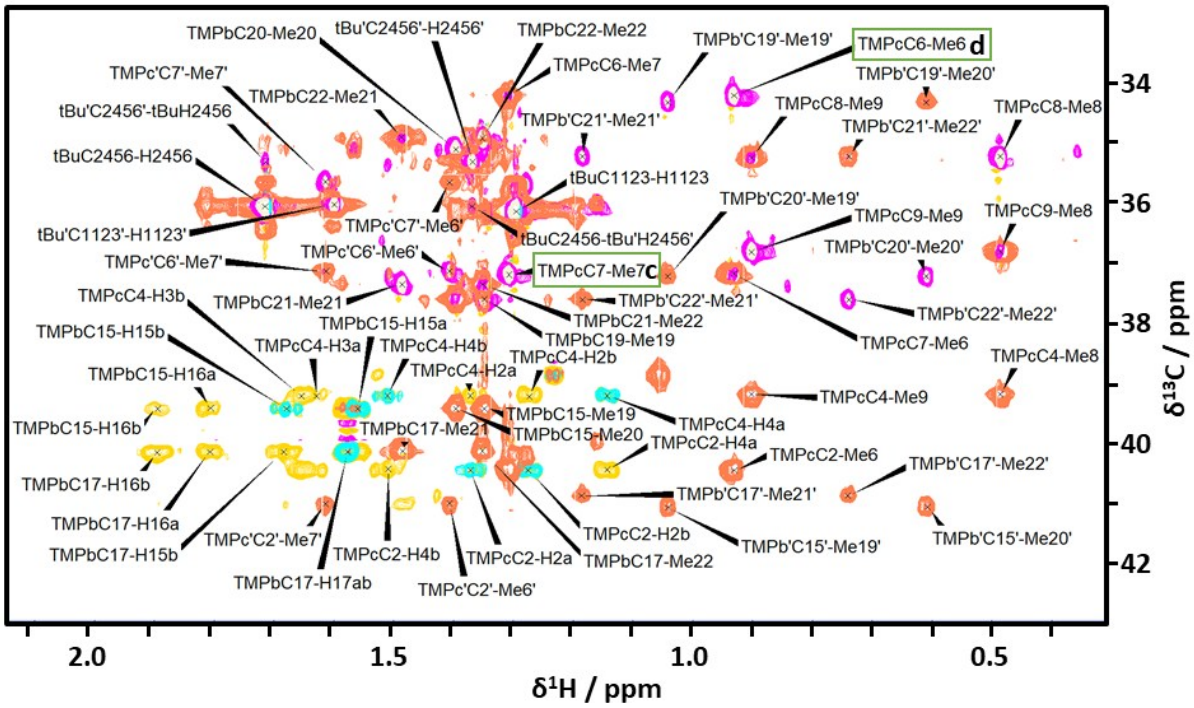

Figure S4 Overlay of part of the 600 MHz 2D [^{1}H, ^{13}C] correlation data of the tetrametallated ferrocene complex **1**. Cross-peaks from a multiplicity-edited 2D [^{1}H, ^{13}C] HSQC NMR data set are colour coded magenta (CH_3/CH groups) and cyan (CH_2 groups). Cross-peaks from a 70 ms 2D [^{1}H, ^{13}C] HSQC-TOCSY NMR data set are colour coded yellow with respect to TMP CH_2 groups. Cross-peaks from a 2D [^{1}H, ^{13}C] HMBC NMR data set are colour coded in buff. Labelling follows the convention F1 assignment (vertical chemical shift scale) δ^{13}C followed by F2 assignment (horizontal chemical shift scale) δ^1H. Cross-peak labels identified inside boxes are referred to in the text by the associated letter with green boxes highlighting selected cross-peak assignments for the "capping" TMP_c units.

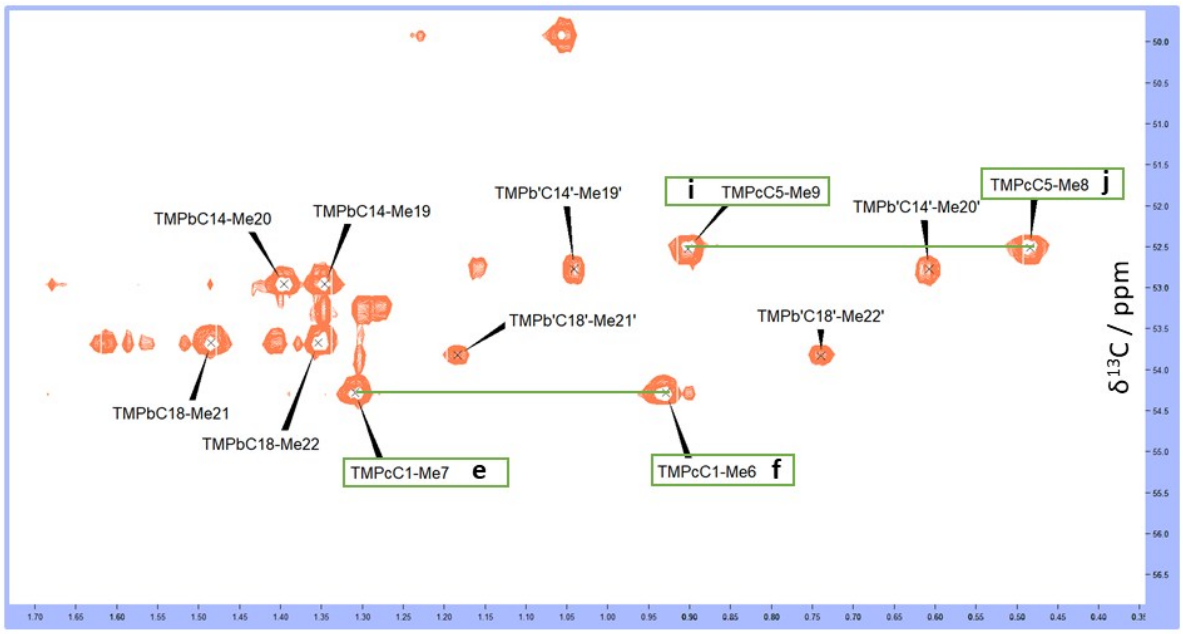

Figure S5 Part of the 600 MHz 2D [^{1}H, ^{13}C] HMBC spectrum of the tetrametallated ferrocene complex **1**. Labelling follows the convention F1 assignment (vertical chemical shift scale) δ^{13}C followed by F2 assignment (horizontal chemical shift scale) δ^{1}H. Cross-peak labels identified inside boxes are referred to in the text by the associated letter with green boxes highlighting selected cross-peak assignments for the "capping" TMP$_c$ units. Green tie-bars indicate the association of ^{1}H NMR resonances from different TMP$_c$ methyl groups to the resonances of the same quaternary carbons to which the methyls are bound. The figure highlights the identity of the ^{1}H NMR resonances for the four methyl groups associated with "capping" TMP$_c$ groups. Inspection of the data also shows identification of the ^{1}H NMR resonances for the methyl groups of the "bridging" TMP$_b$ groups. Cross-peaks assignments showing a prime (') refer to the minor form of the complex (e.g. TMPb'C18'-Me22' expands to a correlation between TMP$_b$C18 and the protons of Methyl 22 in the minor form of the complex).

Examination of the shape of the 2D [^{1}H, ^{13}C] HSQC NMR signals associated with the resonances at δ^{1}H 0.902 and 0.486 ppm revealed these to belong to TMP methyl groups. By inspection of 2D [^{1}H, ^{13}C] HSQC-TOCSY, 2D [^{1}H, ^{13}C] HMBC and pure shift 2D [^{1}H, ^{1}H] TOCSY NMR data, it became clear that the four resonances for methyl groups appearing at δ^{1}H 1.307, 0.931, 0.902 and 0.486 ppm were associated with the same TMP ring. Furthermore, nOe evidence revealed a strong, through-space correlation between two of these four resonances (namely signals at δ^{1}H 0.931 and 0.486 ppm). In the absence of any nOe correlation between

the remaining two methyl groups of this cluster, it was possible to assign the nOe-related methyls to two axially disposed groups not attached to the same quaternary carbon centres but belonging to the same TMP ring. Re-examination of the proton nOe data, including signal intensity evaluation, between the signals of this cluster of methyl groups and the Cp proton resonances, revealed that these data fitted a stereo-specific assignment. The nOe at chemical shift coordinates δ^1H (1.307, 3.746) ppm (cross-peak "**a**" in Figure S3) corresponded to through-space interaction between CpH30 and the methyl labelled 7 in the capping-type TMP$_c$ groups (see Figure S2 for labelling and numbering scheme). By association, the nOe at proton chemical shift coordinates δ^1H (4.228, 0.902) ppm (cross-peak "**h**" in Figure S3) could be assigned to TMP$_c$Me9 and its near Cp proton neighbour, which by inspection of the crystal structure, was found to be CpH27. This critical step in the data analysis was the second major key to opening up the remaining assignments of the major conformational form of the complex. A further set of nOes between CpH30 and a completely different cluster of methyl groups allowed for stereo-specific assignments to be made for the methyl groups of TMP$_b$. In particular, it was possible to stereo-specifically assign TMP$_b$Me21 and TMP$_b$Me22 in relatively similar spatial proximity to CpH30 and giving rise to similar nOe signal intensities at proton chemical shift coordinates δ^1H (3.746, 1.486) ppm (Figure S3, highlighted cross-peak labelled "**k**") and δ^1H (3.746, 1.352) ppm (Figure S3, highlighted cross-peak labelled "**l**") respectively. Similar nOe evidence as that used to assign the TMP$_c$ axially disposed methyl groups was found for the methyl groups of TMP$_b$, thereby allowing completion of the stereo-specific assignment of all methyl groups on both types of TMP ring of the major form of the complex. These assignments were extended to stereo-specific assignment of the protons around the remainder of each TMP ring of the major form of the complex using the nOe evidence to best effect, being consistent with chair conformations of the six-membered rings in each case. Extension of the ^{1}H NMR signal assignment to the associated carbon framework fell out of the data analysis as a matter of course. Full signal assignment for these TMP and Cp components along with specific assignment of the *t*Bu groups of the complex are reported in Table S1. A complete list of all the assigned correlations from 2D [^{1}H, ^{1}H] and 2D [^{1}H, ^{13}C] correlation data sets used in the signal assignment process are reported in Tables S2 and S3 respectively. Using the crystal structure of the major form of the complex also allowed extension of these assignments to be made to each of the two types of *t*Bu groups based on nOe evidence to adjacent, assigned protons associated with the assigned TMP and Cp rings.

Through these means it was possible to complete, as far as was practicable, the assignment of all NMR resonances arising from the major form of the complex as reported in Table S1. The key decision point in this process concerning the relationship between signals and their association with specific rings was based on a chemical shift argument. In particular, it was clear that the two differing types of TMP ring (capping and bridging) gave rise to distinctly different sets of methyl chemical shifts. Thus, TMP_cMe8 and TMP_cMe9 gave rise to proton NMR resonances at lower chemical shifts (δ^1H 0.486 and 0.902 ppm respectively) compared with any of the methyl groups of the TMP_b ring (average δ^1H = 1.396 ppm, σ = 0.056 ppm). This argument was used to place TMP_cMe8 and TMP_cMe9 in comparatively magnetically shielded locations. Logically, this allowed the signal assignments to be made to those methyl groups located above the Cp ring plane, where greater magnetic shielding would be expected. This contrasts with the positions of methyl groups associated with each TMP_b ring, located more proximally adjacent to the plane of the Cp ring. The assignment decision based on this argument was born out by the remaining features of the data, in particular the nOe evidence. Given the strength of this evidence, it was possible to migrate the assignments directly onto the minor form of the complex where possible, by chemical exchange mapping arising from the 2D [^{1}H, ^{1}H] EXSY NMR data (negative cross-peaks, in-phase with the data diagonal peaks). This process was more straightforward for some parts of the data than for others. Difficulties in this translation were mainly due to a combination of lower intensity signals for the minor form of the complex and extensive signal degeneracy within the aliphatic proton resonance region of the data. A summary of the signal assignments available for the minor form of the complex is also detailed in Table S1.

From these data, changes in ^{1}H and ^{13}C chemical shifts were visualized graphically as shown in Figures S6 and S7 respectively. Due to a lack of nOe information associated with the minor form of the complex, it was difficult to draw any conclusions about the actual structure that this complex represents. However, the observed changes in chemical shift, particularly for the proton resonances, are intriguing. Of particular note are the large changes in chemical shift that exist for TMP_bMe20 and TMP_bMe22 ($\Delta\delta^1$H = 0.788 ppm and 0.612 ppm to lower chemical shift respectively) whilst deshielding occurs for TMP_cMe6 and TMP_cMe7 ($\Delta\delta^1$H = 0.476 ppm and 0.308 ppm to higher chemical shift respectively). This indicates some significant rearrangement of the structure in which the TMP_b rings stack above the Cp rings and the TMP_c rings assemble in a planar fashion adjacent to the Cp rings. Consistent with this was the

emergence of some particularly striking information from the exchange data that speculatively provides evidence for a mechanism by which the apparent chemical exchange might occur with a nod towards an insight into the manner by which the complex operates chemically.

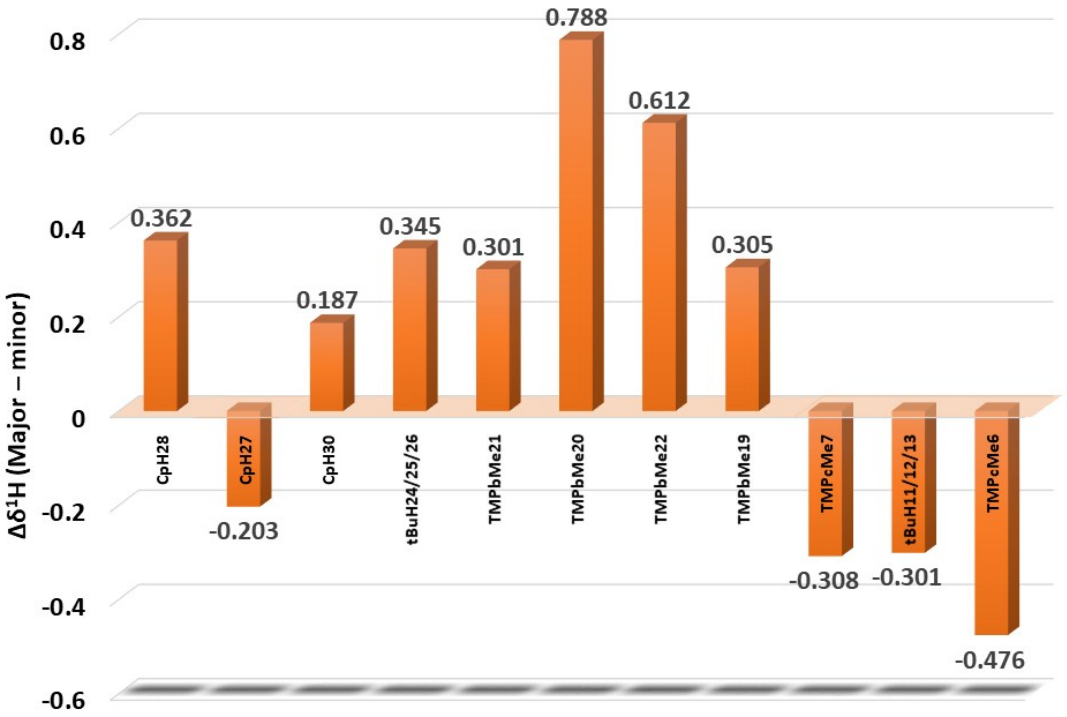

Figure S6 Graphical representation of differences in ^{1}H chemical shift for selected resonances associated with identity-exchanging groups of the major and minor forms of the tetrametallated ferrocene complex **1** presented as $\Delta\delta^{1}$H(major – minor). Positive values indicate groups in the minor form transitioning to more magnetically shielded environments; negative values indicate groups in the minor form transitioning to more magnetically deshielded environments.

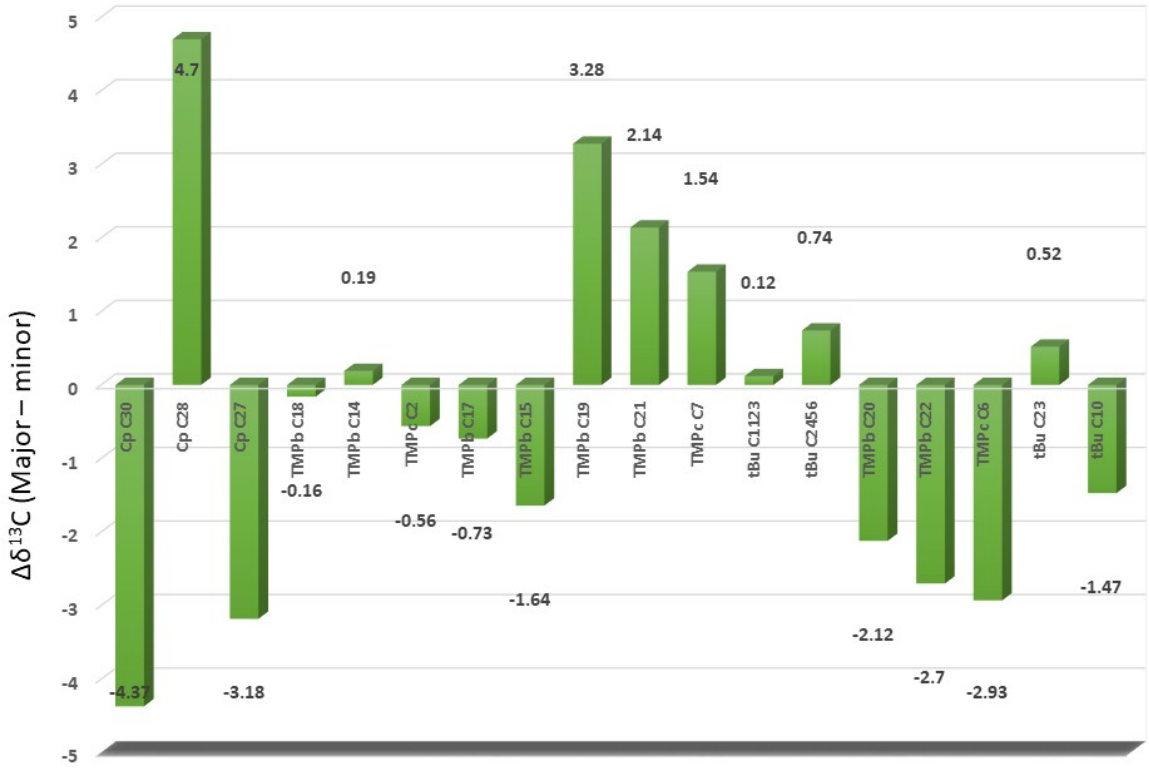

Figure S7 Graphical representation of differences in ^{13}C chemical shift for selected resonances associated with identity-exchanging groups of the major and minor forms of the tetrametallated ferrocene complex presented as $\Delta\delta^{13}C$(major – minor). Positive values indicate groups in the minor form transitioning to more magnetically shielded environments; negative values indicate groups in the minor form transitioning to more magnetically deshielded environments.

The particular features of note in the 2D [^1H, ^1H] EXSY NMR data were exchange cross-peaks that could be clearly assigned to the identity exchange of specific methyl groups belonging to different types of TMP rings ***in the major form of the complex***. Hence, it was possible to assign exchange cross-peaks at chemical shift coordinates corresponding to TMP_cMe8 with TMP_bMe22, TMP_cMe6 with TMP_bMe20 and TMP_cMe9 with TMP_bMe21 (see Figure S8). All of these are associated with the major form of the complex. In other words, the identity of capping and bridging groups clearly interchange. This was also supported by the presence of a chemical exchange cross-peak occurring between the resonances for CpH27 and CpH28 (Figure S9). Taken together, a logical interpretation of this information, given the handedness

of the major form of the complex, is the concerted exchange of capping TMP rings with bridging TMP rings in a twisting fashion which produces the complex with opposing handedness (i.e. the mirror image form). With this in mind, scope exists to consider an intermediate (i.e. the minor form of the complex) existing as a unique species, present with a relatively long lifetime (and therefore observable by NMR) as a half-way transition point between the oppositely handed major forms of the complex. Such an explanation may help to uncover how the chemistry of this complex is performed in the solution phase.

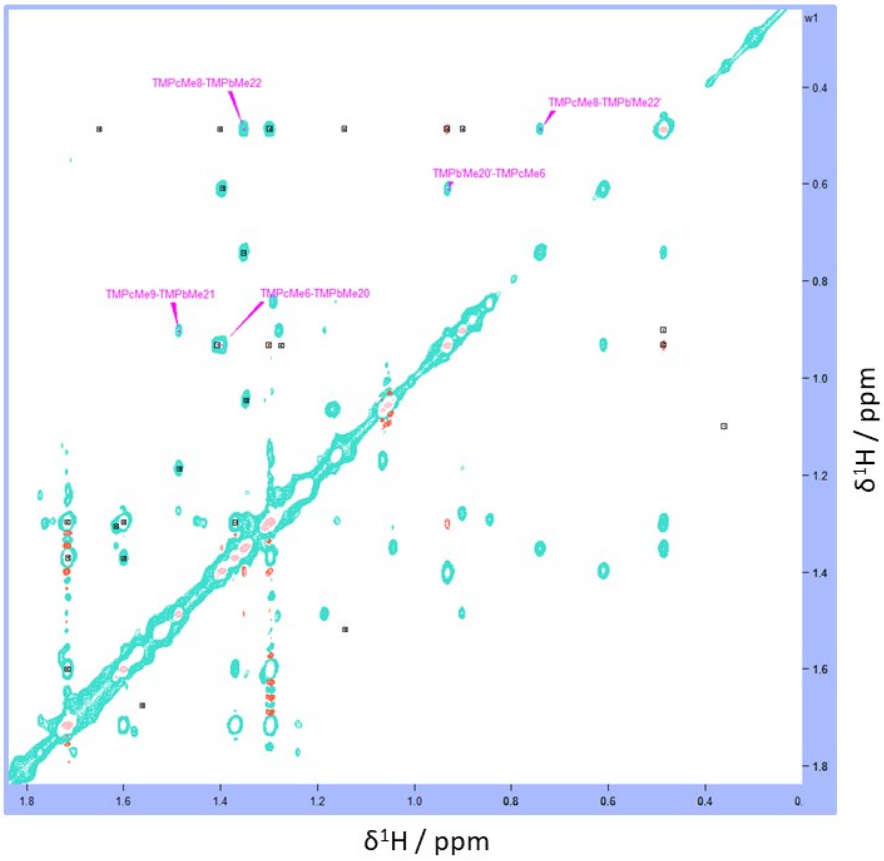

Figure S8 Key region of the 600 MHz 2D [^{1}H, ^{1}H] EXSY/NOESY spectrum from the tetrametallated ferrocene complex **1** in C_6D_6. Highlighted exchange cross-peaks indicate the rearrangement of the major structure to a structurally identical, but oppositely handed form, as well as between major and minor forms.

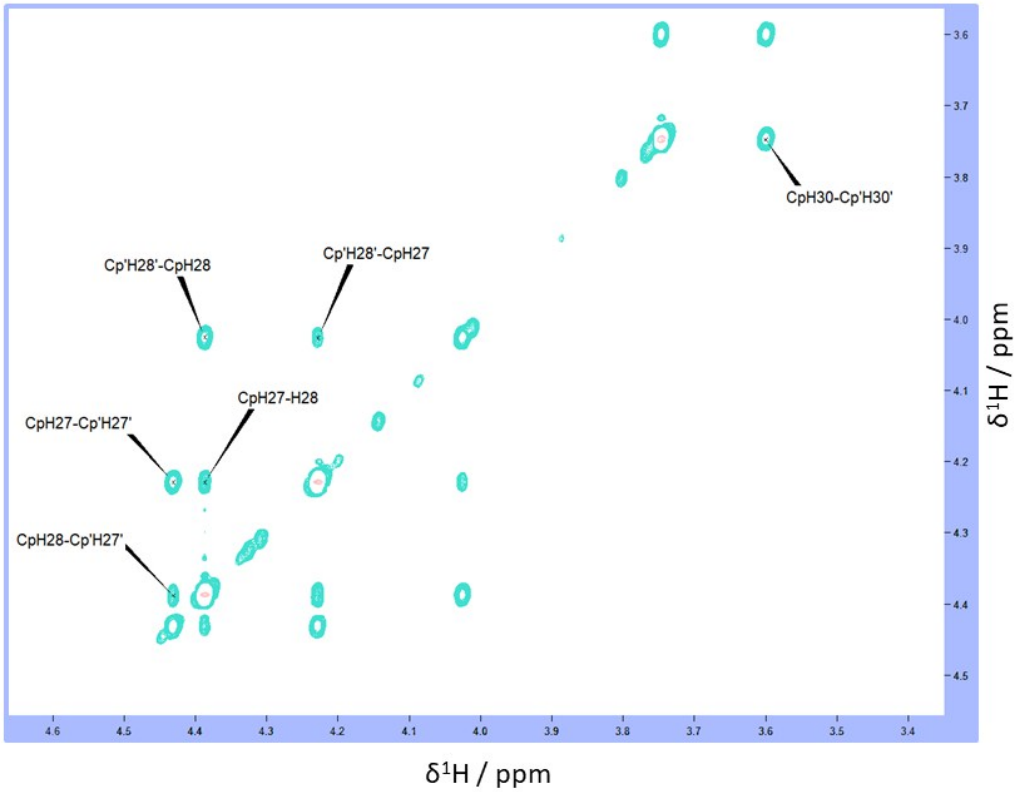

Figure S9 Cp resonance region of the 600 MHz 2D [^{1}H, ^{1}H] EXSY/NOESY spectrum from the tetrametallated ferrocene complex **1** in C_6D_6. Highlighted exchange cross-peaks indicate a major rearrangement of the major structure to a structurally identical, but oppositely handed form, as well as between major and minor forms.

To support this explanation, the exchange rates were calculated using the available 2D [^{1}H, ^{1}H] EXSY NMR data and are summarized in Figure S10.

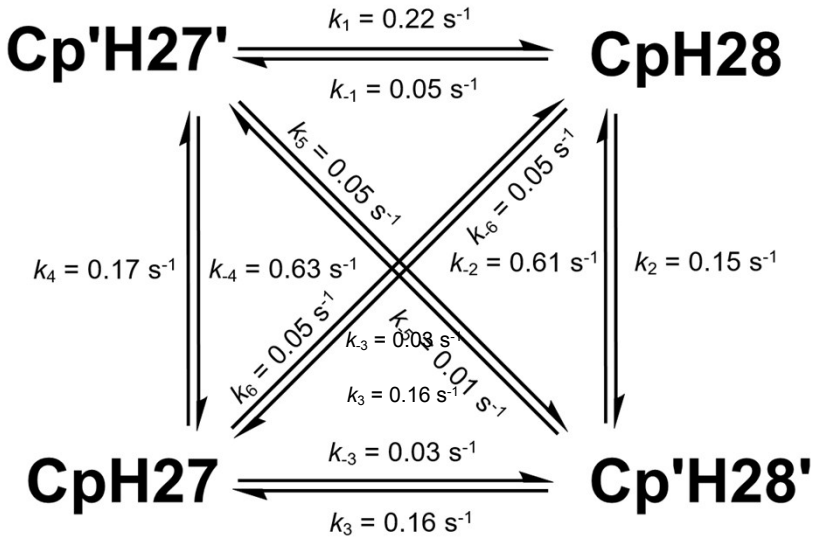

Figure S10 Summary of exchange rate data based on the four-site exchange between Cp protons H27 and H28 in major and minor (primed,') forms of the tetrametallated ferrocene complex.

Extrapolating these data to a qualitative explanation, the figures indicate that the minor form of the complex has a shorter lifetime compared with the major form. Once formed, it has a preference to fall back to the major form from which it emerged (k_{-2} = 0.61 s^{-1}, k_{-4} = 0.63 s^{-1}, ostensibly the same value for the same process). Once present, however, the minor form can instead convert to the oppositely handed major form (k_3 = 0.16 s^{-1}, k_1 = 0.22 s^{-1}) whereby the identities of CpH27 and CpH28 are interconverted. The apparent effect of the major form "twisting" between its mirror image twins is therefore deceptive as shown by the slow rate of interconversion between these structures (k_6 = k_{-6} = 0.05 s^{-1}). The true nature of the interconversion mechanism is a transition which goes *via* the minor form of the complex. Since there is insufficient information in the NMR data to define the structure of the minor form, one can only speculate over this based on the chemical shift information revealed through the assignment process. Using these data, a transition structure can be proposed that would be consistent with an "opening" mechanism in which the TMP and *t*Bu groups relocate into quite different magnetic environments, after which the structure "closes" into either the same handed or the oppositely handed major form of the complex.

Table S1 ^{1}H and ^{13}C chemical shift assignments for the tetrametallated ferrocene complex **1** based on 2D [^{1}H, ^{1}H] and 2D [^{1}H, ^{13}C] correlation NMR data.

Group[a]									
Cp		TMP_b		TMP_c		*t*Bu		*t*Bu	
Atom Number	**$\delta^{13}C$ / ppm**	**Atom Number**	**$\delta^{13}C$ / ppm**	**Atom Number**	**$\delta^{13}C$ / ppm**	**Atom Number**	**$\delta^{13}C$ / ppm**	**Atom Number**	**$\delta^{13}C$ / ppm**
C27	78.58[b]	C14	52.96	C1	54.28	C10	19.66	C23	20.87
	(81.76)[c]		(52.77)				(21.13)		(20.35)
C28	80.10	C15	39.47	C2	40.49	$\underline{C}H_3$ C11/12/13	36.18	$\underline{C}H_3$ C24/25/26	36.09
	(75.40)		(41.11)		(41.05)		(36.06)		(35.35)
C29	88.05	C16	20.23	C3	19.89				
C30	83.30	C17	40.19	C4	39.25				
	(87.67)		(40.92)						
C31	89.58	C18	53.67	C5	52.52				
			(53.83)						
		C19	37.64	C6	34.25				
			(34.36)		(37.18)				
		C20	35.14	C7	37.23				
			(37.26)		(35.69)				
		C21	37.40	C8	35.27				
			(35.26)						
		C22	34.95	C9	36.85				
			(37.65)						
	$\delta^{1}H$ / ppm		**$\delta^{1}H$ / ppm**		**$\delta^{1}H$ / ppm**		**$\delta^{1}H$ / ppm**		**$\delta^{1}H$ / ppm**
H27	4.228	H15a	1.561	H2a	1.371	$C\underline{H}_3$ H11/12/13	1.298	$C\underline{H}_3$ H24/25/26	1.715
	(4.431)						(1.599)		(1.370)
H28	4.387	H15b	1.680	H2b	1.274				
	(4.025)								
H30	3.746	H16a	1.805	H3a	1.630				
	(3.599)								
		H16b	1.897	H3b	1.654				
		H17a	1.577	H4a	1.143				
		H17b	1.577	H4b	1.513				
		$CH_3$19	1.347	$CH_3$6	0.931				
			(1.042)		(1.407)				
		$CH_3$20	1.397	$CH_3$7	1.307				
			(0.609)		(1.615)				
		$CH_3$21	1.486	$CH_3$8	0.486				
			(1.185)						
		$CH_3$22	1.352	$CH_3$9	0.902				
			(0.740)						

a – Groups are colour coded according to the key in Figure S2. b – Values without parentheses correspond to those associated with the major form of the complex. c – Values in parentheses correspond to those assignments associated with the minor form of the complex when observed.

Table S2 Cross-peak assignments for signals associated with the 2D [^{1}H, ^{1}H] EXSY/NOESY NMR data of the tetrametallated ferrocene complex

Cross-Peak Assignment	Coordinates (δ^1H / ppm)		Type[a]
	ω_1	ω_2	
Cp(H27-H28)	4.229	4.387	N
CpH27-Cp'H27'[b]	4.229	4.431	X
CpH28-Cp'H27'	4.388	4.431	X
CpH28-TMP$_b$Me19	4.386	1.348	N
CpH30-Cp'H30'	3.748	3.600	X
CpH30-TMP$_b$Me21	3.746	1.486	N
CpH30-TMP$_b$Me22	3.746	1.352	N
CpH30-TMP$_c$Me7	3.746	1.307	N
CpH30-tBuH11/12/13	3.746	1.296	N
Cp'H28'-CpH27	4.026	4.228	X
Cp'H28'-CpH28	4.025	4.387	X
TMP$_b$(H15b-H15a)	1.675	1.561	N
TMP$_b$(H16a-H16b)	1.801	1.902	N
TMP$_b$Me19-CpH28	1.347	4.388	N
TMP$_b$(Me20-H16b)	1.399	1.899	N
TMP$_b$Me21-CpH30	1.487	3.747	N
TMP$_b$Me22-CpH30	1.352	3.747	N
TMP$_b$(Me22-H16b)	1.353	1.901	N
TMP$_{b'}$Me19'-TMP$_b$Me19	1.046	1.347	X
TMP$_{b'}$Me20'-TMP$_b$Me20	0.609	1.396	X
TMP$_{b'}$Me20'-TMP$_c$Me6	0.610	0.930	X
TMP$_{b'}$Me21'-TMP$_b$Me21	1.187	1.485	X
TMP$_{b'}$Me22'-TMP$_b$Me22	0.742	1.352	X
TMP$_c$(H4b-H4a)	1.518	1.143	N
TMP$_c$Me6-CpH30	0.930	3.747	N
TMP$_c$Me6-TMP$_b$Me20	0.932	1.397	X
TMP$_c$(Me6-H2b)	0.933	1.275	N
TMP$_c$(Me6-Me8)	0.931	0.487	N
TMP$_c$Me6-TMP$_{c'}$Me6'	0.932	1.407	X
TMP$_c$Me6-tBuH11/12/13	0.932	1.301	N
TMP$_c$Me7-CpH30	1.307	3.746	N
TMP$_c$Me7-TMP$_{c'}$Me7'	1.306	1.615	X
TMP$_c$Me8-CpH27	0.485	4.228	N
TMP$_c$Me8-TMP$_b$Me20	0.487	1.401	X
TMP$_c$Me8-TMP$_b$Me22	0.486	1.352	X
TMP$_c$Me8-TMP$_{b'}$Me22'	0.486	0.740	X
TMP$_c$(Me8-H3b)	0.487	1.650	N
TMP$_c$(Me8-H4a)	0.486	1.145	N
TMP$_c$(Me8-Me6)	0.486	0.933	N
TMP$_c$(Me8-Me9)	0.486	0.901	N
TMP$_c$Me9-CpH27	0.902	4.227	N
TMP$_c$Me9-TMP$_b$Me21	0.903	1.486	X
TMP$_c$(Me9-Me8)	0.901	0.487	N
TMP$_{c'}$Me6'-Cp'H28'	1.407	4.027	N
TMP$_{c'}$Me7'-Cp'H28'	1.617	4.025	N
tBuH11/12/13-CpH30	1.301	3.747	N
tBuH11/12/13-Cp'H30'	1.298	3.601	X
tBuH11/12/13-tBuH24/25/26	1.297	1.716	X
tBuH11/12/13-tBu'H11'/12'/13'	1.297	1.600	X
tBuH11/12/13-tBu'H24'/25'/26'	1.298	1.370	X
tBuH24/25/26-CpH27	1.716	4.229	N
tBuH24/25/26-CpH28	1.716	4.387	N
tBu'H11'/12'/13'-Cp'H30'	1.600	3.600	N
tBu'H11'/12'/13'-tBuH24/25/26	1.600	1.716	X
tBu'H24'/25'/26'-Cp'H27'	1.369	4.432	N
tBu'H24'/25'/26'-tBuH24/25/26	1.371	1.715	X
tBu'H24'/25'/26'-tBuH11'/12'/13'	1.372	1.600	X

a – N = nOe cross-peak; X = chemical exchange cross-peak. b – Prime (') indicates association with the minor form identity of the complex

Table S3 Cross-peak assignments for signals associated with 2D [^{1}H, ^{13}C] correlation NMR data of the tetrametallated ferrocene complex.

Cross-peak Assignment	Chemical Shift Coordinates	
	δ^{13}C / ppm, ω_1	δ^{1}H / ppm, ω_2
Cp(C27-H27)	78.580	4.228
Cp(C27-H28)	78.578	4.386
Cp(C27-H30)	78.578	3.746
Cp(C28-H27)	80.102	4.228
Cp(C28-H28)	80.098	4.386
Cp(C28-H30)	80.102	3.746
Cp(C29-H27)	88.060	4.227
Cp(C29-H28)	88.060	4.385
Cp(C29-H30)	88.060	3.745
CpC29-tBuH24/25/26	88.037	1.717
Cp(C30-H27)	83.305	4.227
Cp(C30-H28)	83.293	4.386
Cp(C30-H30)	83.297	3.747
Cp(C31-H27)	89.573	4.227
Cp(C31-H30)	89.596	3.745
CpC31-tBuH11/12/13	89.573	1.297
Cp'(C27'-H27')[b]	81.757	4.431
Cp'(C27'-H28')	81.757	4.023
Cp'(C27'-H30')	81.757	3.598
Cp'(C28'-H27')	75.388	4.431
Cp'(C28'-H28')	75.411	4.026
Cp'(C28'-H30')	75.394	3.599
Cp'(C30'-H27')	87.676	4.430
Cp'(C30'-H28')	87.676	4.022
Cp'(C30'-H30')	87.665	3.598
TMP_b(C14-Me19)	52.956	1.346
TMP_b(C14-Me20)	52.956	1.396
TMP_b(C15-H15a)	39.470	1.560
TMP_b(C15-H15b)	39.470	1.679
TMP_b(C15-H16a)	39.458	1.806
TMP_b(C15-H16b)	39.470	1.894
TMP_b(C15-Me19)	39.468	1.348
TMP_b(C15-Me20)	39.468	1.396
TMP_b(C16-H15b)	20.231	1.680
TMP_b(C16-H16a)	20.225	1.806
TMP_b(C16-H16b)	20.225	1.890
TMP_b(C17-H15b)	40.187	1.684
TMP_b(C17-H16a)	40.187	1.807
TMP_b(C17-H16b)	40.200	1.895
TMP_b(C17-H17a/b)	40.187	1.577
TMP_b(C17-Me21)	40.181	1.485
TMP_b(C17-Me22)	40.174	1.352
TMP_b(C18-Me21)	53.673	1.485
TMP_b(C18-Me22)	53.673	1.354
TMP_b(C19-Me19)	37.639	1.348
TMP_b(C20-Me20)	35.144	1.396
TMP_b(C21-Me21)	37.397	1.486
TMP_b(C21-Me22)	37.400	1.351
TMP_b(C22-Me21)	34.940	1.487
TMP_b(C22-Me22)	34.959	1.352
$TMP_{b'}$(C14'-Me19')	52.774	1.041
$TMP_{b'}$(C14'-Me20')	52.774	0.607
$TMP_{b'}$(C15'-Me19')	41.120	1.041
$TMP_{b'}$(C15'-Me20')	41.108	0.608
$TMP_{b'}$(C17'-Me21')	40.923	1.186
$TMP_{b'}$(C17'-Me22')	40.923	0.741
$TMP_{b'}$(C18'-Me21')	53.822	1.184

$TMP_{b'}$(C18'-Me22')	53.832	0.740
$TMP_{b'}$(C19'-Me19')	34.359	1.042
$TMP_{b'}$(C19'-Me20')	34.359	0.610
$TMP_{b'}$(C20'-Me19')	37.264	1.042
$TMP_{b'}$(C20'-Me20')	37.264	0.610
$TMP_{b'}$(C21'-Me21')	35.262	1.184
$TMP_{b'}$(C21'-Me22')	35.262	0.739
$TMP_{b'}$(C22'-Me21')	37.647	1.184
$TMP_{b'}$(C22'-Me22')	37.647	0.739
TMP_{c}(C1-Me6)	54.279	0.929
TMP_{c}(C1-Me7)	54.279	1.309
TMP_{c}(C2-H2a)	40.495	1.372
TMP_{c}(C2-H2b)	40.495	1.275
TMP_{c}(C2-H4a)	40.484	1.143
TMP_{c}(C2-H4b)	40.472	1.509
TMP_{c}(C2-Me6)	40.495	0.931
TMP_{c}(C3-H2a)	19.885	1.368
TMP_{c}(C3-H2b)	19.897	1.272
TMP_{c}(C3-H3a)	19.885	1.631
TMP_{c}(C3-H3b)	19.885	1.659
TMP_{c}(C3-H4a)	19.897	1.142
TMP_{c}(C3-H4b)	19.885	1.513
TMP_{c}(C4-H2a)	39.255	1.372
TMP_{c}(C4-H2b)	39.268	1.273
TMP_{c}(C4-H3a)	39.260	1.629
TMP_{c}(C4-H3b)	39.260	1.654
TMP_{c}(C4-H4a)	39.255	1.143
TMP_{c}(C4-H4b)	39.255	1.510
TMP_{c}(C4-Me8)	39.231	0.486
TMP_{c}(C4-Me9)	39.231	0.902
TMP_{c}(C5-Me8)	52.512	0.484
TMP_{c}(C5-Me9)	52.530	0.902
TMP_{c}(C6-Me6)	34.245	0.931
TMP_{c}(C6-Me7)	34.248	1.309
TMP_{c}(C7-Me6)	37.222	0.931
TMP_{c}(C7-Me7)	37.234	1.307
TMP_{c}(C8-Me8)	35.261	0.486
TMP_{c}(C8-Me9)	35.285	0.902
TMP_{c}(C9-Me8)	36.844	0.486
TMP_{c}(C9-Me9)	36.856	0.902
$TMP_{c'}$(C2'-Me6')	41.046	1.407
$TMP_{c'}$(C2'-Me7')	41.059	1.614
$TMP_{c'}$(C6'-Me6')	37.177	1.407
$TMP_{c'}$(C6'-Me7')	37.177	1.613
$TMP_{c'}$(C7'-Me6')	35.694	1.407
$TMP_{c'}$(C7'-Me7')	35.682	1.614
tBu(C10-H11/12/13)	19.659	1.298
tBu(C11/12/13-H11/12/13)	36.179	1.295
tBu(C23-H24/25/26)	20.874	1.714
tBu(C24/25/26-H24/25/26)	36.096	1.715
tBuC24/25/26-tBu'H24'/25'/26'	36.093	1.369
tBu'(C10'-H11'/12'/13')	21.127	1.598
tBu'(C11'/12'/13'-H11'/12'/13')	36.062	1.599
tBu'(C23'-H24'/25'/26')	20.349	1.370
tBu'C24'/25'/26'-tBuH24/25/26	35.351	1.714
tBu'(C24'/25'/26'-H24'/25'/26')	35.351	1.368

b – Prime (') indicates association with the minor form identity of the complex

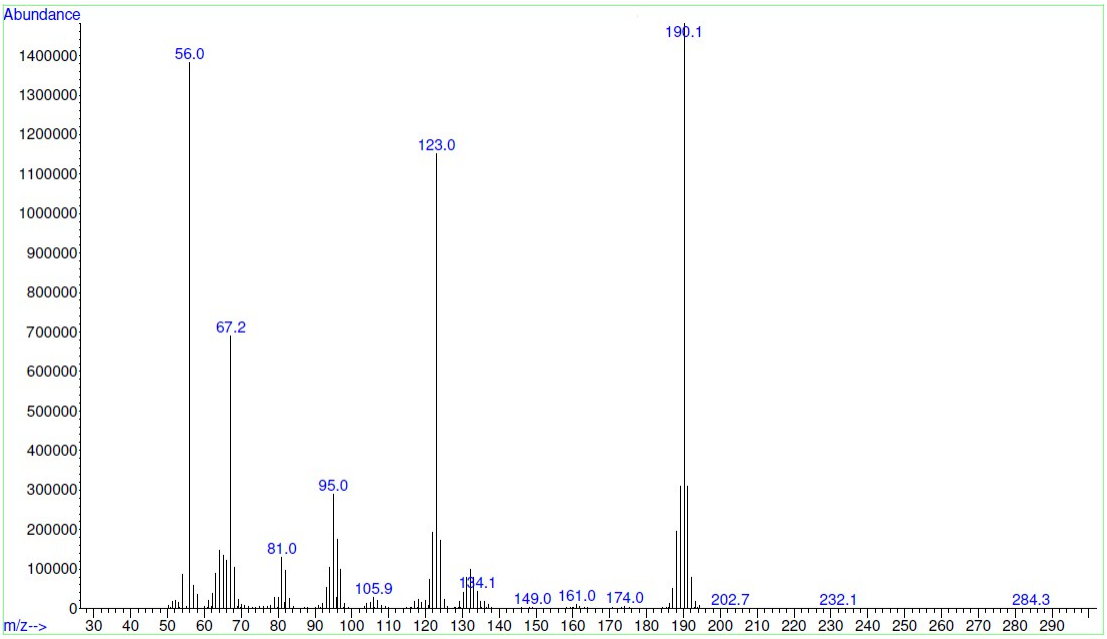

Figure S11 GC-MS spectrum of product of D_2O quench of tetrametallated ferrocene complex **1**

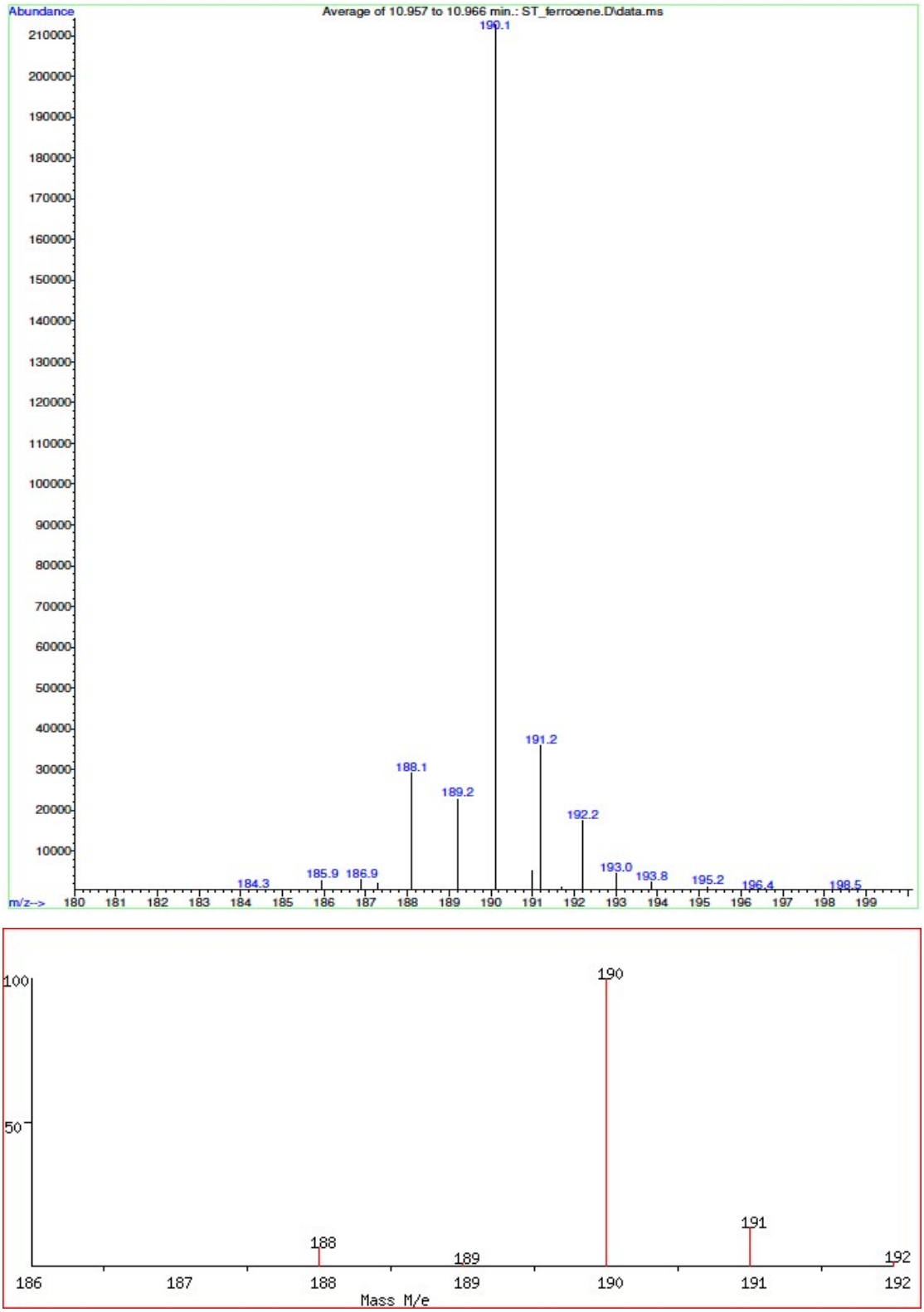

Figure S12 Blow up of GC-MS spectrum of product of D_2O quench of tetrametallated ferrocene complex **1** (top) and the calculated mass spectrum of $Fe(C_5H_3D_2)_2$ (bottom)

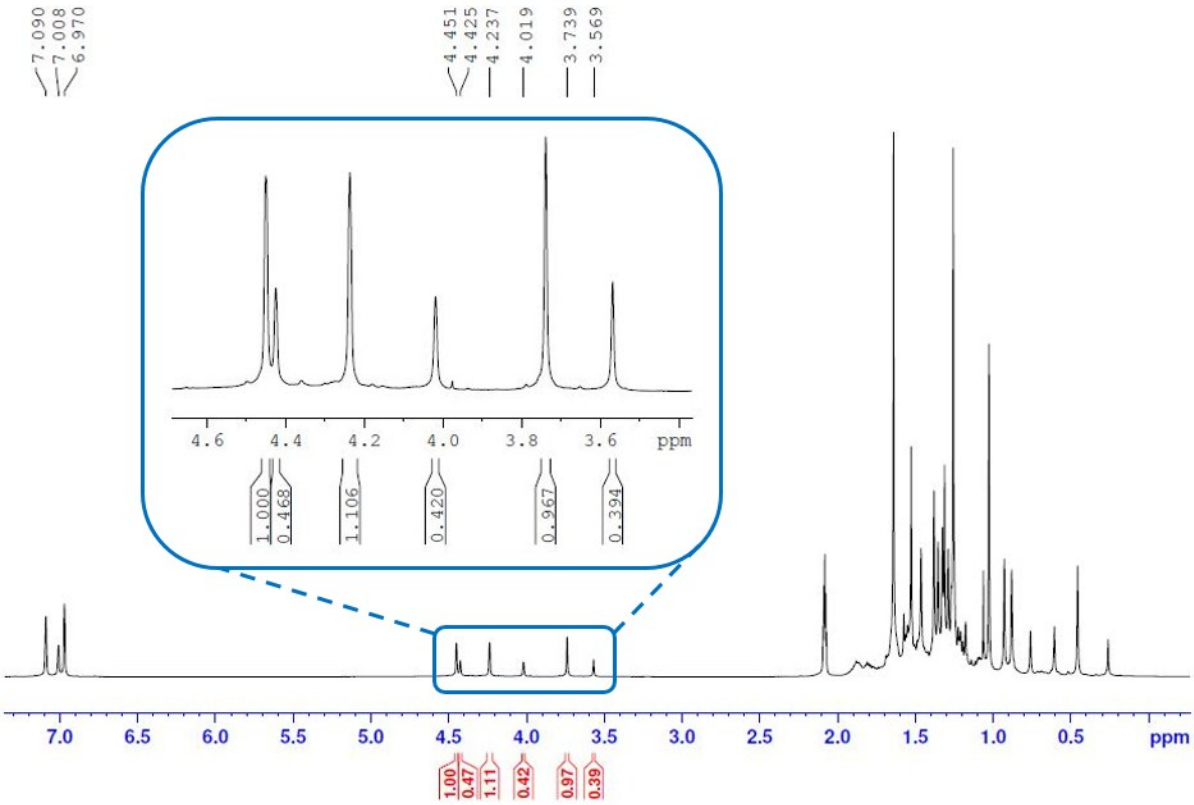

Figure S13 ^{1}H NMR spectrum of complex **2** in C_7D_8

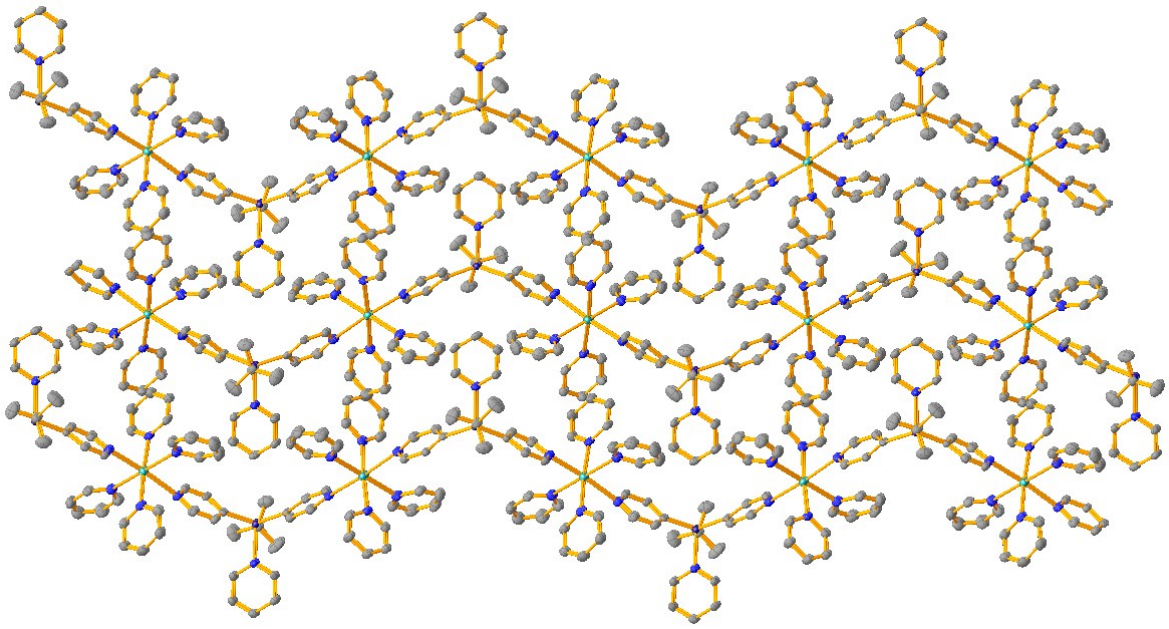

Figure S14 Solid-state packing of complex **3**

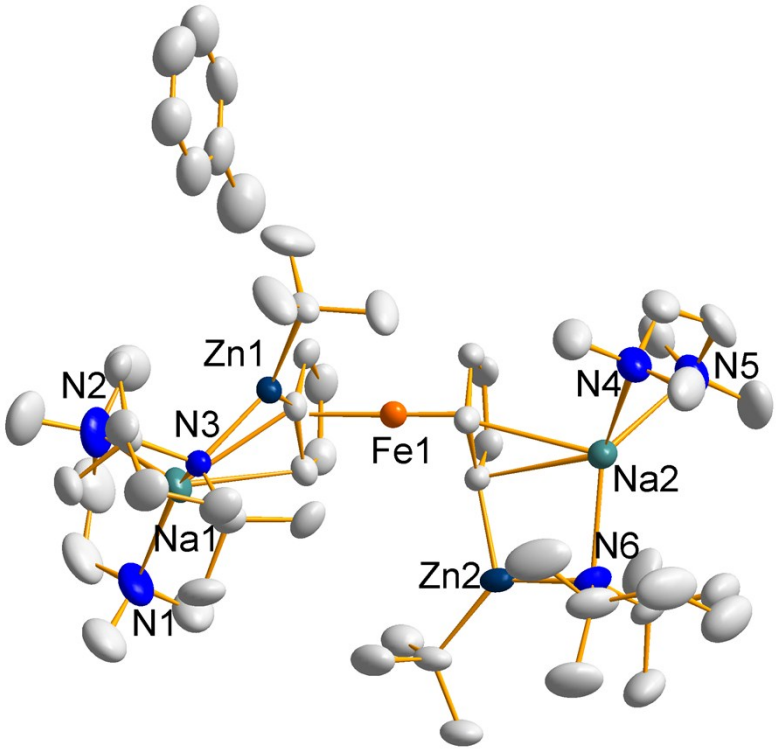

Figure S15 Molecular structure of sodium zincate [TMEDA·Na(μ-TMP)Zn*t*Bu]$_2$(C_5H_4)$_2$Fe·C_7H_8 **(4)**. Ellipsoids are shown at 50% probability and all hydrogen atoms and minor disordered components have been removed for clarity.

Table S4 Crystallographic data and refinement details for complexes **1**-**4**

	1	**2**	**3**	**4**
Empirical formula	$C_{62}H_{114}FeN_4Na_4Zn_4$	$C_{68}H_{110}FeN_4Na_4Zn_4$	$C_{39}H_{42}N_7NaZn$	$C_{55}H_{102}FeN_6Na_2Zn_2$
Mol. Mass	1324.86	1392.88	697.15	1079.99
Crystal system	Monoclinic	Monoclinic	Orthorhombic	Triclinic
Space group	C2/*c*	P2(1)/*c*	P 2(1)2(1)2(1)	P -1
a/Å	27.3950(16)	14.895(2)	8.8556(2)	12.9797(5)
b/Å	44.055(4)	26.966(4)	17.4144(4)	15.0261(6)
c/Å	14.5103(8)	18.622(3)	23.9796(5)	15.9756(8)
α/°	90	90	90	99.482(4)
β/°	100.575(5)	111.871(2)	90	90.798(4)
γ/°	90	90	90	99.459(3)
V/Å^3	17215(2)	6941.3(18)	3698.01(14)	3028.7(2)
Z	10	4	4	2
λ/Å	1.54814	0.6814	1.54814	0.71073
Measured reflections	35626	28486	9912	26552
Unique reflections	16676	8467	6328	14120
R_{int}	0.0414	0.0842	0.0423	0.0275
Observed rflns [$I>2\sigma(I)$]	12197	6099	4534	9836
GooF	1.106	1.043	0.883	1.013
R [on *F*, obs rflns only]	0.1091	0.0778	0.0400	0.0466
ωR [on F^2, all data]	0.2567	0.1859	0.0871	0.1154
Largest diff. peak/hole e/Å^{-3}	1.172/-0.782	1.360/-1.179	0.387/-0.241	0.626/-0.376